

Supporting Information

I- Materials and Methods.

All moisture and oxygen sensitive compounds were prepared using standard vacuum-argon lines, Schlenk and cannula techniques. All reagents were purchased from Aldrich or Acros and used as received, unless noted otherwise. Acetonitrile solvent was purified by distillation under argon over CaH₂. For electrochemical experiments, extra dry acetonitrile was passed over alumina before use, whereas butyronitrile was first passed over silica and then on alumina.

[Fe^{II}(L₅²)(MeCN)](PF₆)₂ (1**)** was prepared as already reported.¹

[Fe^{III}(L₅²)(OOH)](PF₆)₂ was prepared as previously described.^{2,3} [Fe^{III}(OOH)(L₅²)](PF₆)₂ was obtained by reaction of [Fe^{II}Cl(L₅²)](PF₆) (42 mg, 7.2 × 10⁻⁵ mol, 3 mM) with 100 equiv. H₂O₂ (35%) in MeOH (24 mL) at RT. After a few seconds, the resulting purple solution was cooled down to low temperature (-80°C to -90°C) which was maintained during the rest of the procedure. An excess of NaPF₆ (10 equiv., 121 mg) and cold Et₂O (100 mL) were added leading to the precipitation of a purple flocculent solid. The solvent and excess hydrogen peroxide were removed *via* a cannula equipped with a glass filter. The resulting purple [Fe^{III}(OOH)(L₅²)](PF₆)₂ solid was carefully washed with cold Et₂O (3 × 30 mL) and redissolved in cold PrCN. The concentration of the resulting stock solution was determined by considering its LMCT band at 530 nm (1000 M⁻¹cm⁻¹)⁴ and double integration of the S=1/2 EPR signal.

[Fe^{III}(L₅²)(OO)]²⁺ was obtained by deprotonation of [Fe^{III}(L₅²)(OOH)]²⁺ in PrCN at -70°C with 3 equiv. *t*BuOK. As reported by Simaan et al.,^{5,6} the purple ([Fe^{III}(L₅²)(OOH)]²⁺) and blue ([Fe^{III}(L₅²)(OO)]⁺) chromophores are subject to a reversible acid/base equilibrium.

[Fe^{IV}(L₅²)(O)](PF₆)₂ was obtained by treatment of **1** with excess solid PhIO in MeCN at RT as described by Bohn et al.¹

NMR spectra were obtained on Bruker 360 MHz or Bruker 300 MHz spectrometers.

Determination of the magnetic moment of [Fe^{II}(L₅²)(MeCN)](PF₆)₂ by the Evans NMR method.⁷

Coaxial NMR tubes were used. The inner capillary tube contained CD₃CN. The outer tube contained the complex (m = 10 mg/mL) in CD₃CN. The paramagnetic shift was measured on the residual CD₃CN peak.

The general formula for the mass susceptibility is: $\chi_g = -3\Delta f / (4\pi Fm) + [\chi^\circ + \chi^\circ(d^\circ - d^s) / m]$

Where m is the mass of complex (in g) in 1 mL of solution, Δf is the separation between the peaks (TMS or CD₃CN) of the inner and outer tubes in Hz, F is the frequency of the spectrometer in Hz (300 MHz), χ° is the susceptibility of the pure solvent, d° the density of the solvent, d^s the density of the complex solution.

In the present case, with a dilute solution (13.6 mM), d^s can be approximated to ($d^\circ + m$) and the expression simplifies to: $\chi_g = -3\Delta f / (4\pi Fm)$

The molar susceptibility is $\chi_M = M \times \chi_g$ and the paramagnetic susceptibility is given by $\chi_{para} = \chi_M - \chi_{dia}$.

The diamagnetic corrections χ_{dia} were determined using Pascal's constants.⁸

X-band EPR spectra were recorded on a Bruker ELEXSYS 500 spectrometer equipped with a Bruker ER 4116DM X band resonator, an Oxford Instrument continuous flow ESR 900 cryostat, and an Oxford ITC 503 temperature control system. Experimental conditions, Perpendicular mode: Microwave frequency 9.65 GHz, microwave power 1.0 mW, modulation amplitude 8 Gauss, gain 50 dB, modulation frequency 100 kHz, 10 K. Quantification of the S = ½ signal was done by fitting the area of the signal to a calibration curve obtained from a series of CuSO₄ solutions in MeOH at different concentrations.

Cyclic Voltammetry experiments were performed using an Autolab potentiostat and a conventional 3-electrode device (glassy carbon working electrode, platinum counter electrode and SCE reference electrode). The electrolyte salt (Bu₄NPF₆) was recrystallized and all the glassware was dried at 110°C before use. All the cyclic voltammograms (CVs) were recorded in acetonitrile solution containing 0.1 M Bu₄NPF₆ at a scan rate of 0.1 V/S. Study of the reaction between complex **1** and O₂ were performed in air saturated acetonitrile at room temperature, *i.e.* at a dioxygen concentration of 1.62 mM.^{9,10} Before any CV of the **1** + O₂ system, background CVs of the solvent with electrolyte salt were realized and compensation of the ohmic drop was ensured.

Normalization of the CVs' intensity with respect to the one at $v_0 = 0.1 \text{ V}\cdot\text{s}^{-1}$ was done using Randles-Sevcik equation for a monoelectronic process :

$$i_p = \left(0.4463 \times F \times A \times [\text{Fe}] \sqrt{\frac{F}{RT}} \right) \sqrt{D} \sqrt{v} = C \sqrt{v}$$

where

i_p = anodic or cathodic current intensity (A) R = ideal gas constant (8.314 J.K⁻¹.mol⁻¹)
 F = Faraday constant (96500 C.mol⁻¹) D = diffusion coefficient (cm².s⁻¹)
 A = electrode surface (0.0707 cm²) v = scan rate (V.s⁻¹)
 $[\text{Fe}]$ = concentration of complex (mol.cm⁻³) T = absolute temperature (K)

Therefore, at $v_0 = 0.1 \text{ V.s}^{-1}$

$$i_0 = C \sqrt{v_0}$$

And at v_1

$$i_1 = C \sqrt{v_1} = C \sqrt{k_1 v_0}$$

Normalization of i_1 , recorded at $v_1 = k_1 v_0$, with respect to $v_0 = 0.1 \text{ V.s}^{-1}$ follows

$$\frac{i_1}{\sqrt{k_1}} = i_1^{norm} = C \sqrt{v_0} = i_0$$

Simulations of the CVs were performed using Digilch program.¹¹ To benchmark the simulations of the **1** + O₂ system, the CVs of the stable species **1**, O₂, and of the chemically prepared [Fe^{III}(L₅²)(OOH)]²⁺ and [Fe^{III}(L₅²)(OO)]⁺ intermediates were preliminary recorded and simulated separately to determine relevant parameters such as standard potentials and electron transfer rate constants.

Electrolyses experiments were performed using a carbon foam working electrode, a platinum grid counter electrode and a SCE reference electrode. The reactants were added as solids to the 0.1 M TBAPF₆ solution (7 mL in acetonitrile) that had been degassed with O₂ for ten minutes at RT. They were added in the following order: [Fe^{II}(L₅²)(MeCN)](PF₆)₂ (1 mM), TBABr (100 equivalents), anisole (100 equivalents), ± H₂O (250 equivalents).

The applied potential was held constant at -650 mV vs SCE for two hours at room temperature while the solution was agitated and bubbled continuously with pure dioxygen (solubility of 8 mM in acetonitrile)¹⁰ that was dried over molecular sieves (4 Å). After 2-hours, the acetonitrile solution was concentrated to 1 mL by rotary evaporation (250 mbar, 35°C). As an internal standard, 3 µL of a 660 mM acetophenone solution was added to the concentrated sample. The sample was then precipitated over 10 mL of diethyl ether, then filtered over 2 cm SiO₂ in a Pasteur pipette and eluted with 2 mL Et₂O. The diethyl ether was then evaporated (850 mbar, 35°C). The residue was retaken in 1 mL of MeCN, then analysed by GC.

Gas Chromatography analyses of the reaction products were performed with a Shimadzu GC-2010 Plus gas chromatograph. Samples were injected in a Zebron ZB Semi Volatiles column (30 m x 0.25 mm x 0.25 µm). The methodology (temperature ramps) is indicated below.

Initial Temperature: 50°C

Equilibration Time: 1 min

Total Program Time: 27 min

Rate (C/min)	Temp.(C)	Hold Time (min)
-----	50.0	5.00
10.00	220.0	5.00

II- Spectroscopic, electrochemical and mechanistic data.

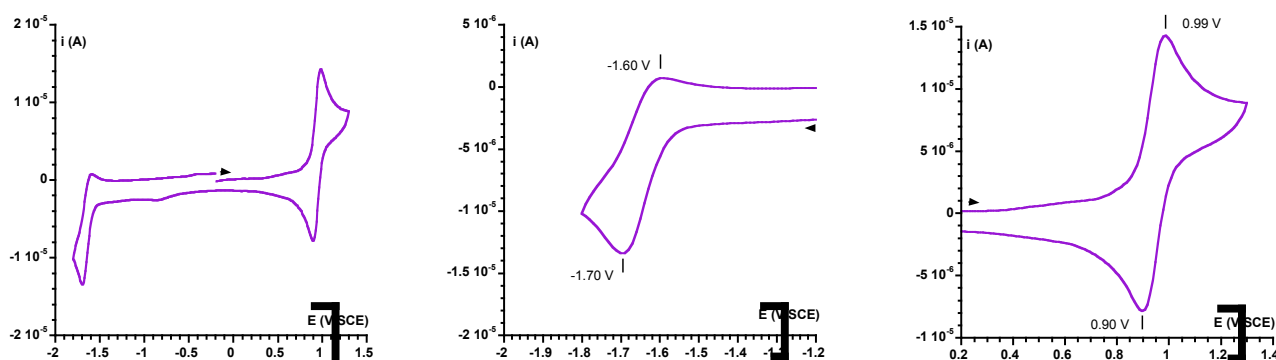


Figure S1. (Left) CV of $[\text{Fe}^{\text{II}}(\text{L}_5^2)(\text{MeCN})]^{2+}$ (**1**) under argon at a scan rate of $0.1 \text{ V}\cdot\text{s}^{-1}$ (1 mM in MeCN, 0.1 M TBAPF₆); (middle) zoom on the Fe^{II}/Fe^I and (right) Fe^{III}/Fe^{II} redox couples. The initial direction of the scan is indicated by an arrow.

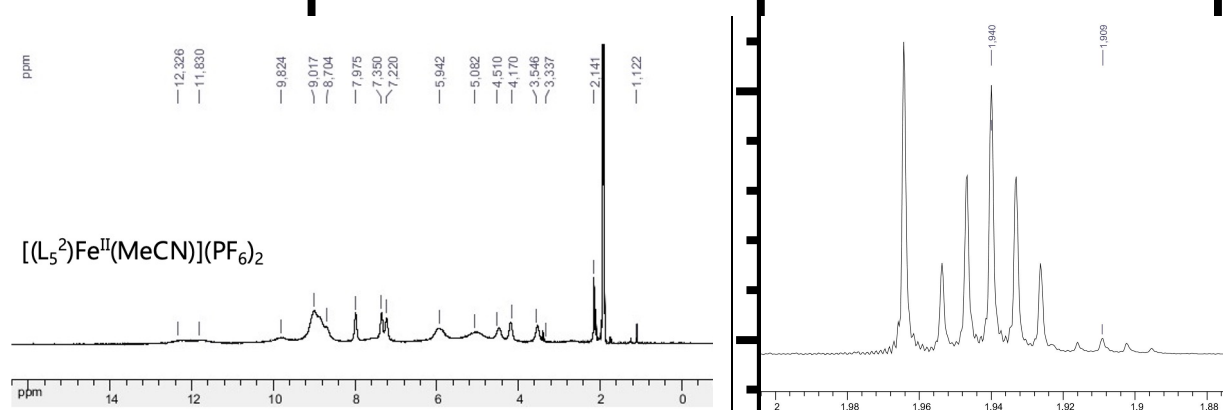
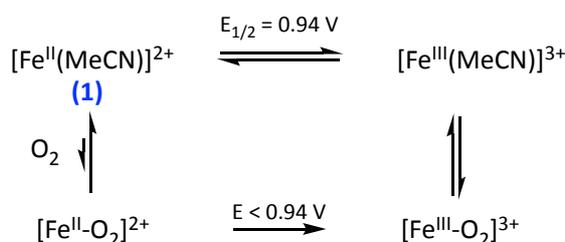


Figure S2. (Left) ¹H NMR spectrum (CD₃CN, 300 K, 360 MHz) of $[\text{Fe}^{\text{II}}(\text{L}_5^2)(\text{MeCN})](\text{PF}_6)_2$. (Right) Zoom to show the shift of the CD₃CN signal used to determine the magnetic moment by Evans method ($\mu_{\text{eff}} = 1.6 \mu_{\text{B}}$; 30% HS).



Scheme S1. Square scheme to rationalize the behaviour of complex **1** in oxygenated acetonitrile solutions. The L₅² ligand has been omitted for simplicity.

The set of cyclic voltammograms in Figure 1 are normalized to a scan rate of $0.1 \text{ V}\cdot\text{s}^{-1}$. That the normalized CVs under O₂ are not superimposable indicates that the concentration of **1** probed at the electrode is dependent on the scan rate: the slower the scan rate, the lower the concentration of **1**. This observation implies that **1** is involved in a chemical equilibrium under O₂ but not under argon (compare Figure 1, B and C). The square scheme above (Scheme S1) provides a rationalization for these observations.

Provided that the coordination of O₂ to the Fe^{II} centre in **1** is slow, the equilibrium for the Fe^{II}-O₂ adduct formation has time to establish only at slow scan rate. Under these conditions, some amount of complex **1** forms the Fe^{II}-O₂ adduct and this amount is not probed at E_{pa} = 0.99 V. As the scan rate increases, there is less and less time for O₂ to substitute the iron-coordinated acetonitrile in **1** and the proportion of **1** detected at 0.99 V progressively increases. Such a mechanistic proposition translates into the representation of the intensity of the anodic peak as a function of the scan rate which increases progressively to reach a maximum value at high scan rate (Figure 1, B). In contrast, the similar representation reveals a constant anodic intensity in the absence of O₂ (Figure 1, C).

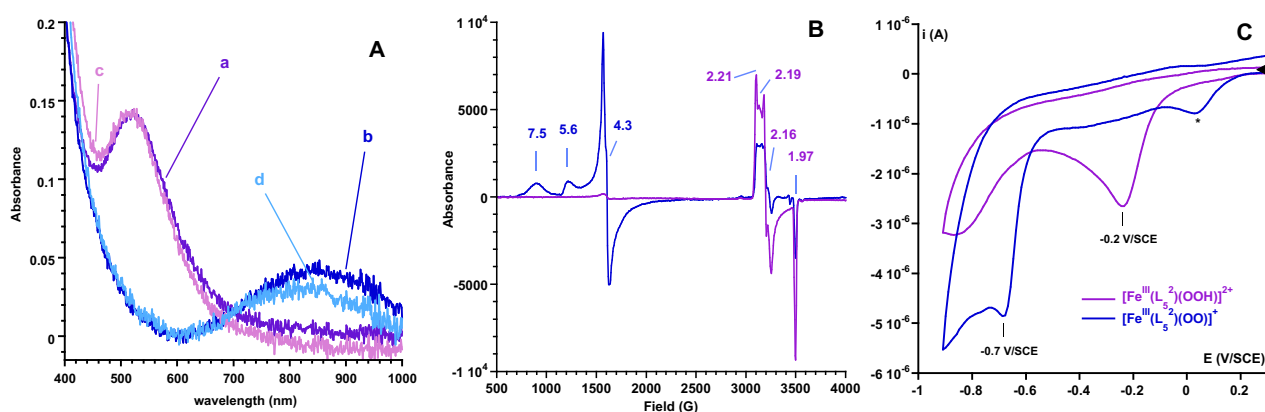


Figure S3. (A) UV-Visible monitoring of the acid/base equilibrium between $[\text{Fe}^{\text{III}}(\text{L}_5^2)(\text{OOH})]^{2+}$ and $[\text{Fe}^{\text{III}}(\text{L}_5^2)(\text{OO})]^+$ in PrCN at -70°C . (a) $[\text{Fe}^{\text{III}}(\text{L}_5^2)(\text{OOH})]^{2+}$ (0.15 mM); (b) $[\text{Fe}^{\text{III}}(\text{L}_5^2)(\text{OO})]^+$ obtained by reaction of $[\text{Fe}^{\text{III}}(\text{L}_5^2)(\text{OOH})]^{2+}$, trace **a**, with 3 equiv. *t*BuOK; (c) $[\text{Fe}^{\text{III}}(\text{L}_5^2)(\text{OOH})]^{2+}$ obtained by reaction of $[\text{Fe}^{\text{III}}(\text{L}_5^2)(\text{OO})]^+$, trace **b**, with 3 equiv. HClO_4 ; (d) $[\text{Fe}^{\text{III}}(\text{L}_5^2)(\text{OO})]^+$ obtained by reaction of $[\text{Fe}^{\text{III}}(\text{L}_5^2)(\text{OOH})]^{2+}$, trace **c**, with 3 equiv. *t*BuOK. (B) X-band EPR spectrum of $[\text{Fe}^{\text{III}}(\text{OOH})(\text{L}_5^2)]^{2+}$ and of the same sample in the presence of *t*BuOK. (C) CV of $[\text{Fe}^{\text{III}}(\text{L}_5^2)(\text{OOH})]^{2+}$ (purple trace) and $[\text{Fe}^{\text{III}}(\text{L}_5^2)(\text{OO})]^+$ (blue trace) recorded in PrCN/0.2 M TBAPF₆ at -70°C . The asterisk denotes for residual oxo-bridged dinuclear species formed due to the instability of the peroxo intermediate and the basic conditions.

UV-visible monitoring reveals that acid/base equilibrium between $[\text{Fe}^{\text{III}}(\text{L}_5^2)(\text{OOH})]^{2+}$ and $[\text{Fe}^{\text{III}}(\text{L}_5^2)(\text{OO})]^+$ is reversible, even though the intermediates are relative unstable under these conditions.

The EPR spectrum of the low spin $[\text{Fe}^{\text{III}}(\text{L}_5^2)(\text{OOH})]^{2+}$ species displays its typical resonances at $g = 2.21/2.19$, 2.16, 1.97.^{1,2} Addition of the base *t*BuOK leads to the decrease of these resonances and appearance of the signature of the high spin $[\text{Fe}^{\text{III}}(\text{L}_5^2)(\text{OO})]^+$ intermediate at $g = 7.5$, 5.6 (the $g = 4.3$ resonance is due to ubiquitous Fe^{III} degradation species). Note that an acid/base equilibrium is temperature dependent. By cooling down to 10 K, the protonation reaction, which is exothermic, is favoured. As such, the reaction progress reverts back by comparison with the UV-visible monitoring at 203 K (panel A) to favour the $\text{Fe}^{\text{III}}(\text{OOH})$ form.

The values of the cathodic peak potential for $[\text{Fe}^{\text{III}}(\text{L}_5^2)(\text{OOH})]^{2+}$ and $[\text{Fe}^{\text{III}}(\text{L}_5^2)(\text{OO})]^+$ have been previously reported by our group.¹² They are consistent with those reported by Ségau et al. for the related intermediates $[\text{Fe}^{\text{III}}(\text{TPEN})(\text{OOH})]^{2+}$ (-0.16 V vs SCE) and $[\text{Fe}^{\text{III}}(\text{TPEN})(\text{OO})]^+$ (-0.58 V vs SCE).⁹

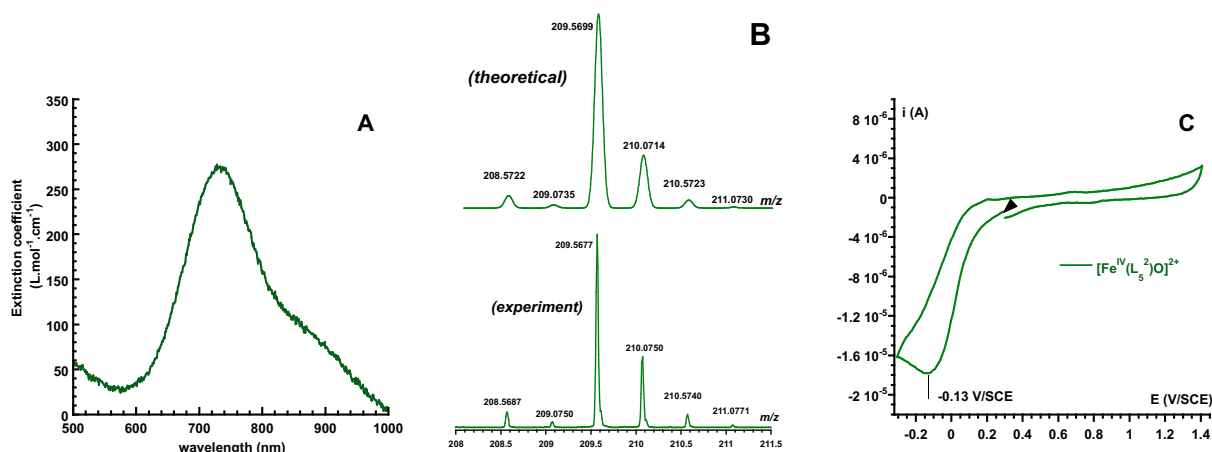


Figure S4. (A) UV-Visible spectrum of $[\text{Fe}^{\text{IV}}(\text{L}_5^2)(\text{O})]^{2+}$ in MeCN at RT. (B) Experimental and theoretical isotope patterns for $\text{Fe}^{\text{IV}}(\text{L}_5^2)\text{O}_2^+$. (C) CV of $[\text{Fe}^{\text{IV}}(\text{L}_5^2)(\text{O})]^{2+}$ recorded at 0.1 V/s in MeCN/0.1 M TBAPF₆ at 0°C .

The value of the cathodic peak potential for $[\text{Fe}^{\text{IV}}(\text{L}_5^2)(\text{O})]^{2+}$ is consistent with those reported by Ségau et al.⁹ and Wang et al.¹³ for a series of related intermediates ($E_{p,c}$ ranging between -0.18 and 0.08 V/SCE).

Mechanism A		
E1	$O_2 + e^- = O_2^{\cdot -}$	$E^\circ = -0.89$ $k^\circ = 0.007$
C1	$[Fe^{II}]^{2+} + O_2 = [Fe^{II}-O_2]^{2+}$	$K_1 = 40$ $k_+ = 1.0 \cdot 10^6$
E2	$[Fe^{III}]^+ + e^- = [Fe^{II}]^{2+}$	$E^\circ = 0.94$ $k^\circ = 0.009$
C2	$[Fe^{II}]^{2+} + O_2^{\cdot -} = [Fe^{II}(O_2^{\cdot -})]^+$	$K_2 = 6.7 \cdot 10^5$ $k_+ = 1.0 \cdot 10^8$
E3	$[Fe^{II}-O_2]^{2+} + e^- = [Fe^{II}(O_2^{\cdot -})]^+$	$E^\circ = -0.64$ $k^\circ = 0.009$
C3	$[Fe^{II}(O_2^{\cdot -})]^+ \rightleftharpoons [Fe^{III}(OO^{\cdot -})]^+$	$K = 1.10^{10}$ $k_+ = 1.0 \cdot 10^{10}$
E4	$[Fe^{III}(OO^{\cdot -})]^+ + e^- \rightleftharpoons [Fe^{II}(OO^{\cdot -})]$	$E^\circ_{app} = -0.7$ $k^\circ = 0.009$
C4	$[Fe^{III}(OO^{\cdot -})]^+ + H_2O = [Fe^{III}(OOH)]^{2+}$	$K_4 = 3.5 \cdot 10^5$ $k_+ = 1.0 \cdot 10^{14}$
E5	$[Fe^{III}(OOH)]^{2+} + e^- \rightleftharpoons [Fe^{II}(OOH)]^+$	$E^\circ = -0.20$ $k^\circ = 0.009$
C5	$[Fe^{II}(OO^{\cdot -})] + H_2O = [Fe^{II}(OOH)]^+$	$K_5 = 1.0 \cdot 10^{14}$ $k_+ = 1.0 \cdot 10^{14}$

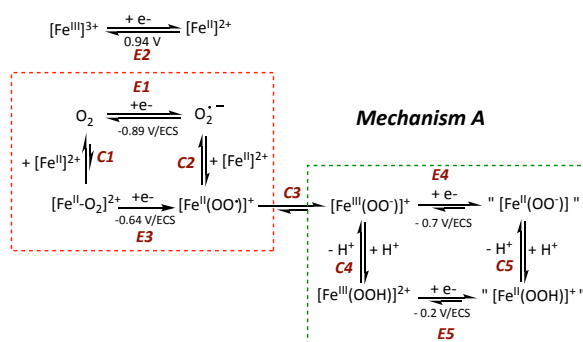


Figure S5. (Left) Chemical (C) and electrochemical (E) reactions taken into account in Mechanism A to simulate the experimental CVs of the **1** + O₂ reaction mixtures. The symbols "=" and "==" stand for equilibrated and irreversible reactions, respectively. E⁰ values are given in V vs SCE, k⁰ are in cm.s⁻¹, k₊ are in M⁻¹.s⁻¹ and K units depend on the reaction order. The underlined parameters have been determined upon optimization of the simulations following iterative processes, the other ones have been determined experimentally, except for reaction C3. (Right) Detailed Mechanism A.

As expected, an adequate simulation (see Figure 2 in the main text) requires that the affinity of **1** for O₂ is much less than for superoxide (compare K₁ and K₂). Also, the optimized K₄ and K₅ values (which are dependent on each other due to the square scheme) indicate that the electron deficient [Fe^{III}(L₅²)(OO)]⁺ is a weaker base than its reduced form [Fe^{II}(L₅²)(OO)]. Reaction C3 occurring between two valence tautomers is considered to be spontaneous and its K and k₊ constants have been fixed accordingly.

Mechanism B		
E1	$O_2 + e^- = O_2^{\cdot-}$	$E^\circ = -0.89$ $k^\circ = 0.007$
C1	$[Fe^{II}]^{2+} + O_2 = [Fe^{II}\text{-}O_2]^{2+}$	$K_1 = 40$ $k_+ = 1.0 \cdot 10^6$
E2	$[Fe^{III}]^{3+} + e^- = [Fe^{II}]^{2+}$	$E^\circ = 0.94$ $k^\circ = 0.009$
C2	$[Fe^{II}]^{2+} + O_2^{\cdot-} = [Fe^{II}(O_2^{\cdot-})]^+$	$K_2 = 6.7 \cdot 10^5$ $k_- = 1.0 \cdot 10^8$
E3	$[Fe^{II}\text{-}O_2]^{2+} + e^- = [Fe^{II}(O_2^{\cdot-})]^+$	$E^\circ = -0.64$ $k^\circ = 0.009$
C3	$[Fe^{II}(O_2^{\cdot-})]^+ \rightleftharpoons [Fe^{III}(OO\cdot)]^+$	$K = 1.10 \cdot 10^{10}$ $k_+ = 1.0 \cdot 10^{10}$
E4	$[Fe^{III}(OO\cdot)]^+ + e^- \rightleftharpoons [Fe^{II}(OO\cdot)]$	$E^\circ_{app} = -0.7$ $k^\circ = 0.009$
C4	$[Fe^{III}(OO\cdot)]^+ + H_2O = [Fe^{III}(OOH)]^{2+}$	$K_4 = 3.5 \cdot 10^5$ $k_+ = 1.0 \cdot 10^{14}$
E5	$[Fe^{III}(OOH)]^{2+} + e^- \rightleftharpoons [Fe^{II}(OOH)]^+$	$E^\circ = -0.20$ $k^\circ = 0.009$
C5	$[Fe^{II}(OO\cdot)] + H_2O = [Fe^{II}(OOH)]^+$	$K_5 = 1.0 \cdot 10^{14}$ $k_+ = 1.0 \cdot 10^{14}$
C6	$[Fe^{II}(OOH)]^+ + [Fe^{II}(OOH)]^+ \rightleftharpoons A + O_2$	$K_6 = 1.0 \cdot 10^{10}$ $k_+ = 1.0 \cdot 10^{10}$
C7	$A \rightleftharpoons [Fe^{II}(OH)]^+ + [Fe^{III}(OH)]^+$	$K_7 = 1.0 \cdot 10^{10}$ $k_+ = 1.0 \cdot 10^{16}$

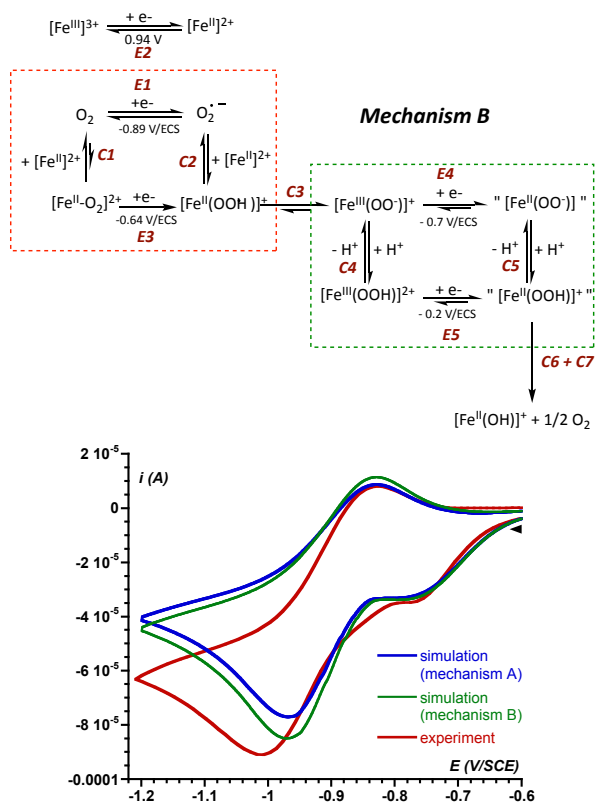


Figure S6. (Left) Chemical (C) and electrochemical (E) reactions applied in Mechanism B to simulate the experimental CVs of the **1** + O₂ reaction mixtures. The symbols "=" and "=>" stand for equilibrated and irreversible reactions, respectively. E⁰ values are given in V vs SCE, k⁰ are in cm²·s⁻¹, k₊ are in M⁻¹·s⁻¹ and K units depend on the reaction order. The underlined parameters have been determined upon optimization of the simulations following iterative processes, the other ones have been determined experimentally, except for reaction C3. Disproportionation of the [Fe^{II}(OOH)]⁺ has been decomposed into C6 + C7 since DigiElch software does not take into account stoichiometric coefficients other than 1. (Right) Detailed Mechanism B. The resulting CV simulation is shown as the green curve and compared to the CV simulated with Mechanism A and the experimental one.

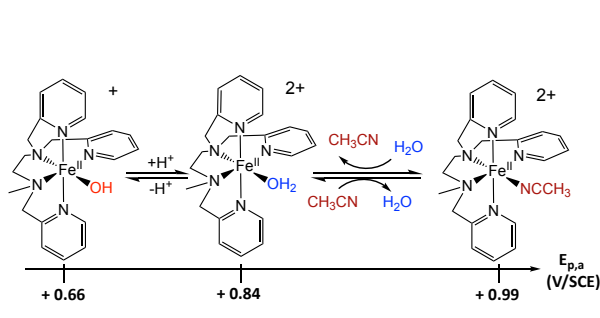
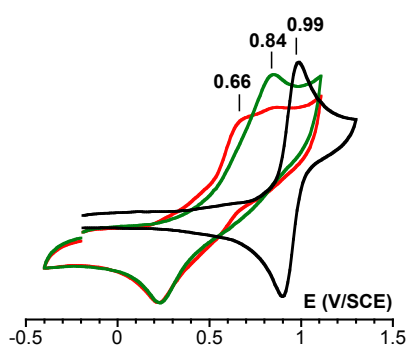


Figure S7. CVs of [Fe^{II}(L₅²)(MeCN)]²⁺ (**1**) in dry degassed MeCN (black trace); in MeCN/H₂O (75/25 v/v) (green trace); and in MeCN/H₂O (75/25 v/v) after addition of tBuOK (0.2 equiv. vs Fe) (red trace). T=20°C, 0.1 V·s⁻¹, 0.1 M TBAPF₆. The anodic peak of **1** is shifted from 0.99 to 0.84 V in the presence of water and further to 0.66 V when a base is added. The peak at 0.84 V can thus be assigned to [Fe^{II}(L₅²)(OH₂)]²⁺, whereas the peak at 0.66 V is ascribed to [Fe^{II}(L₅²)(OH)]⁺; as summarized on the right panel.

Mechanism C		
E1	$O_2 + e^- = O_2^{\cdot-}$	$E^\circ = -0.89$ $k^0 = 0.007$
C1	$[Fe^{II}]^{2+} + O_2 = [Fe^{II}-O_2]^{2+}$	$K_1 = 40$ $k_+ = 1.0 \cdot 10^6$
E2	$[Fe^{III}]^+ + e^- = [Fe^{II}]^{2+}$	$E^\circ = 0.94$ $k^0 = 0.009$
C2	$[Fe^{II}]^{2+} + O_2^{\cdot-} = [Fe^{II}(O_2^{\cdot-})]^+$	$K_2 = 6.7 \cdot 10^5$ $k_+ = 1.0 \cdot 10^8$
E3	$[Fe^{II}-O_2]^{2+} + e^- = [Fe^{II}(O_2^{\cdot-})]^+$	$E^\circ = -0.64$ $k^0 = 0.009$
C3	$[Fe^{II}(O_2^{\cdot-})]^+ \rightleftharpoons [Fe^{III}(OO\cdot)]^+$	$K = 1.10^{10}$ $k_+ = 1.0 \cdot 10^{10}$
E4	$[Fe^{III}(OO\cdot)]^+ + e^- \rightleftharpoons [Fe^{II}(OO\cdot)]$	$E^\circ_{app} = -0.7$ $k^0 = 0.009$
C4	$[Fe^{III}(OO\cdot)]^+ + H_2O = [Fe^{III}(OOH)]^{2+}$	$K_4 = 3.5 \cdot 10^5$ $k_+ = 1.0 \cdot 10^{14}$
E5	$[Fe^{III}(OOH)]^{2+} + e^- \rightleftharpoons [Fe^{II}(OOH)]^+$	$E^\circ = -0.20$ $k^0 = 0.009$
C5	$[Fe^{II}(OO\cdot)] + H_2O = [Fe^{II}(OOH)]^+$	$K_5 = 1.0 \cdot 10^{14}$ $k_+ = 1.0 \cdot 10^{14}$
C6	$[Fe^{II}(OOH)]^+ + [Fe^{II}(OOH)]^+ \rightleftharpoons A + O_2$	$K_6 = 1.0 \cdot 10^{10}$ $k_+ = 1.0 \cdot 10^{10}$
C7	$A \rightleftharpoons [Fe^{II}(OH)]^+ + [Fe^{II}(OH)]^+$	$K_7 = 1.0 \cdot 10^{10}$ $k_+ = 1.0 \cdot 10^{16}$
E6	$[Fe^{III}(OH)]^{2+} + e^- = [Fe^{II}(OH)]^+$	$E^\circ = 0.81$ $k^0 = 0.009$
C8	$[Fe^{III}(OO\cdot)]^+ + O_2^{\cdot-} = [Fe^{II}(OO\cdot)]$	$K_8 = 1.6 \cdot 10^3$ $k_+ = 500$
C9	$[Fe^{III}(OOH)]^{2+} + O_2^{\cdot-} = [Fe^{II}(OOH)]^+$	$K_9 = 4.6 \cdot 10^{11}$ $k_+ = 500$
C10	$[Fe^{II}]^{2+} + H_2O = [Fe^{II}(OH)]^+$	$K_{10} = 50$ $k_+ = 100$
C11	$[Fe^{III}]^{3+} + H_2O = [Fe^{III}(OH)]^{2+}$	$K_{11} = 4.6 \cdot 10^{11}$ $k_+ = 500$

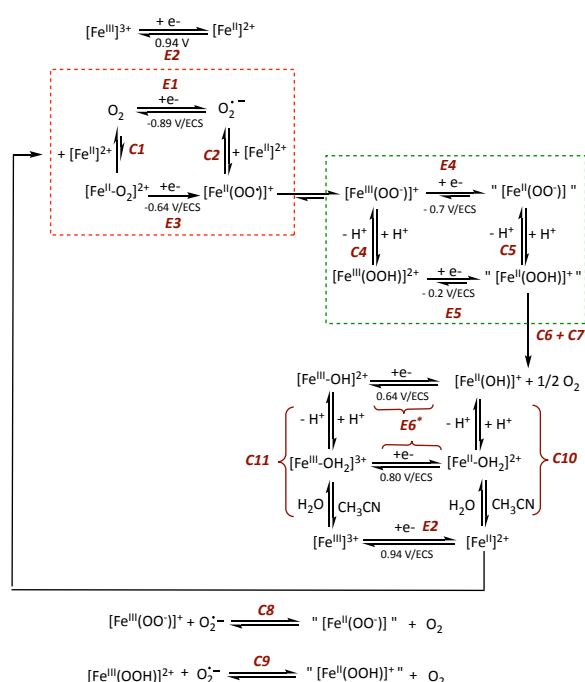


Figure S8. (Left) Chemical (C) and electrochemical (E) reactions applied in Mechanism C to simulate the experimental CVs of the **1** + O₂ mixtures. The symbols "=" and "=>" stand for equilibrated and irreversible reactions, respectively. E⁰ values are given in V vs SCE, k⁰ are in cm.s⁻¹, k₊ are in M⁻¹.s⁻¹ and K units depend on the reaction order. The underlined parameters have been determined upon optimization of the simulations following iterative processes, the other ones have been determined experimentally, except for reaction C3. Disproportionation of the [Fe^{II}(OOH)]⁺ has been decomposed into C6 + C7 since DigiElch software does not consider stoichiometric coefficients other than 1. The equilibria between the Fe^{III/II}(NCCH₃), Fe^{III/II}(OH₂) and Fe^{III/II}(OH) have been merged into a single phenomenological reaction between Fe^{III/II}(NCCH₃) and Fe^{III/II}(OH) for the sake of simplification (C10 and C11). For the same reason, redox reactions have been restricted to two Fe^{III}/Fe^{II} couples (E2 and E6).

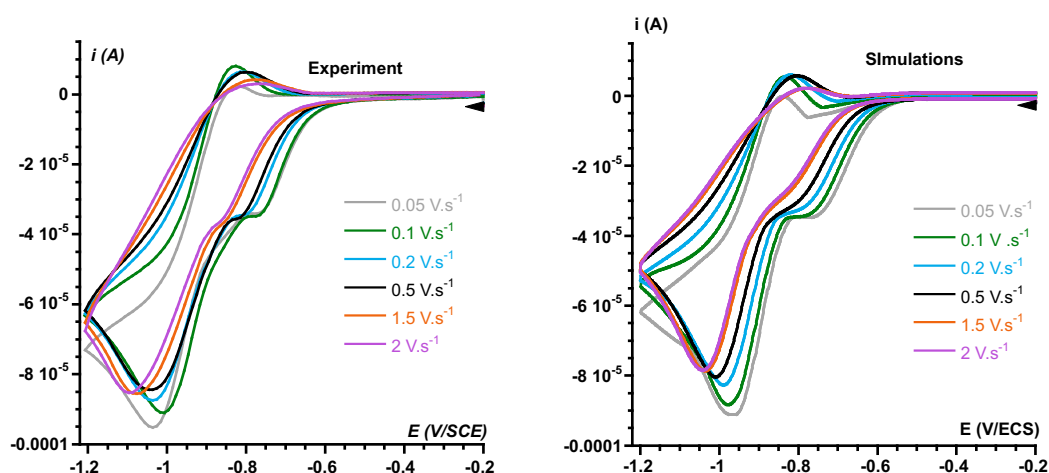


Figure S9. CVs and simulations of an equimolar mixture of **1** (1.6 mM) and O_2 in dry CH_3CN at room temperature and various scan rates (as indicated). The shift of the plateau-shaped wave at -0.70 V towards more negative potentials as the scan rate increases and the progressive loss in intensity and reversibility of the $O_2/O_2^{\bullet-}$ wave are satisfactorily simulated.

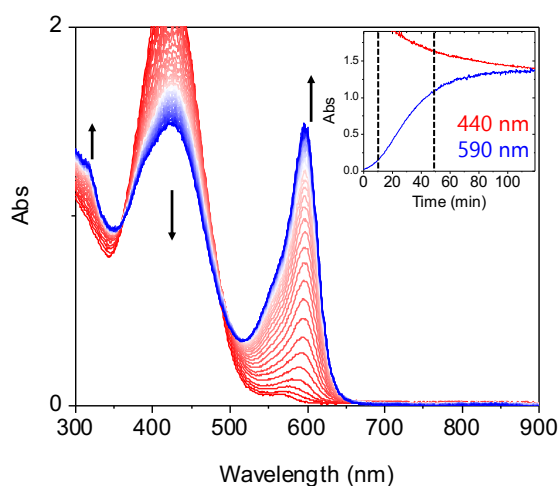


Figure S10. Evolution of the UV-vis spectrum during the conversion of phenol red (67 μM) to bromophenol blue in the presence of **1** (0.1 mM) and TBABr (80 mM) after the addition of H_2O_2 (10 mM) in methanol under ambient atmosphere. Insert shows the change in time of the 440 nm chromophore (phenol red) and the 590 nm chromophore (bromophenol blue). Control experiments by systematically removing one of the reactants did not yield bromophenol blue.

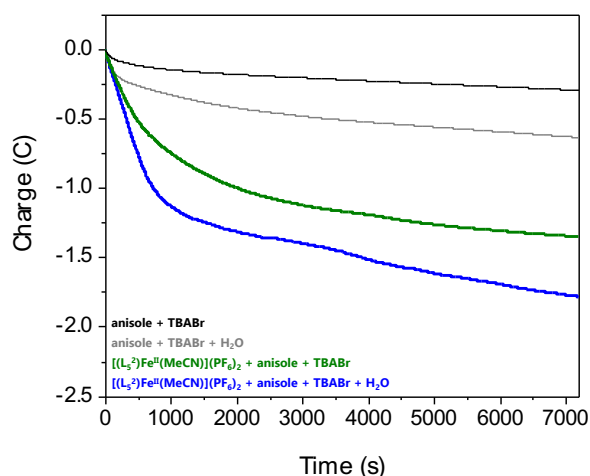


Figure S11. Plots of the charge accumulated during the electrolysis experiments. Each experiment was followed for 2 hours in MeCN at RT with the application of a constant potential at -650 mV, and 0.1 M TBAPF₆ used as supporting electrolyte. Conditions for each plot: Blue: 1 mM **1**, 100 mM anisole, 100 mM TBABr, and 250 mM H_2O ; Green: 1 mM **1**, 100 mM anisole, and 100 mM TBABr; Grey: 100 mM anisole, 100 mM TBABr, and 250 mM H_2O ; Black: 100 mM anisole and 100 mM TBABr.

III- CV simulations.

Simulations of the CVs require to consider the following parameters for electrochemical reactions

$D(\text{species})$: diffusion coefficient of the species

$E^0(\text{couple})$: standard potential of the redox couple, referred to SCE

k^0 : rate constant of the heterogenous electron transfer

α : transfer coefficient of the electron transfer = 0.5 in any case.

For chemical reactions, the parameters to consider are

k_+ : rate constant of the direct reaction

$K = k_+/k_-$: equilibrium constant of the reaction

When possible, *i.e.* for stable species and chemically prepared reaction intermediates, the electrochemical parameters were determined following CV analyses and simulations, as detailed below. The parameters obtained were then used for the simulations of the CVs of **1** in the presence of O_2 .

For chemical reactions, the values of the thermodynamic and kinetic constants were validated when satisfying simulation of the experimental CVs were obtained and provided that they are not aberrant.

Chemical reactions involving water were taken into account when simulating the CVs of **1** in the presence of O_2 . A concentration in residual water of 2 mM was found convenient to properly reproduce the shape and intensity of the intensity-potential curves.

For the simulations of the **1** + O_2 reaction mixtures, the initial concentration of these reactants was indicated while it was set to zero for any other species (except for water, see above). For the simulations of the reaction intermediates CVs, their initial concentration was indicated while it was set to zero for any other species (except for water, see above).

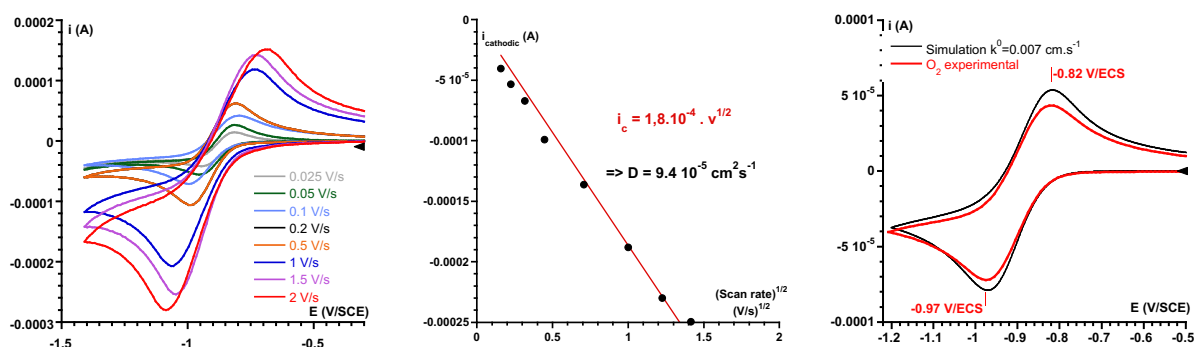


Figure S12. (Left) CV of O_2 (1.6 mM in extra dry MeCN, 0.1 M TBAPF₆) at 20°C at various scan rates at a glassy carbon electrode. (Middle) Determination of the diffusion coefficient using Randles-Sevcik equation. (Right) Simulation of the CV at 0.1 Vs⁻¹ with $E^0(O_2/O_2^{\cdot-}) = -0.89$ V, $k^0 = 0.007$ cm.s⁻¹, $D(O_2) = 9.4 \cdot 10^{-5}$ cm²s⁻¹.

The value of the D coefficient obtained for O_2 is consistent with the one determined by Ségau et al. ($9.0 \cdot 10^{-5}$ cm²s⁻¹).⁷ For the CV simulations of the **1** + O_2 reaction mixtures, this value has been used for $O_2^{\cdot-}$ as well.

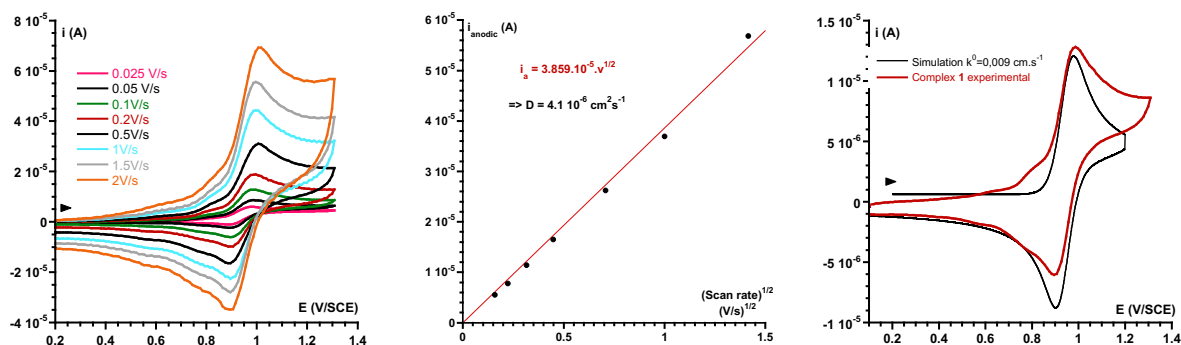


Figure S13. (Left) CV of complex **1** (1 mM in extra dry MeCN, 0.1 M TBAPF₆) at 20°C at various scan rates at a glassy carbon electrode. (Middle) Determination of the diffusion coefficient using Randles-Sevcik equation. (Right) Simulation of the CV at 0.1 V.s⁻¹ with E⁰(Fe^{III}/Fe^{II}) = 0.94 V, k⁰ = 0.009 cm.s⁻¹, D(**1**) = 4.1 10⁻⁶ cm².s⁻¹.

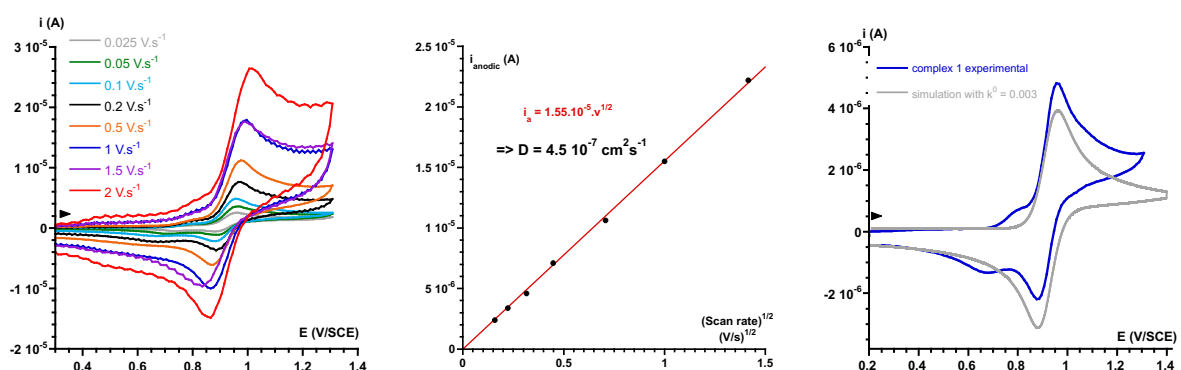
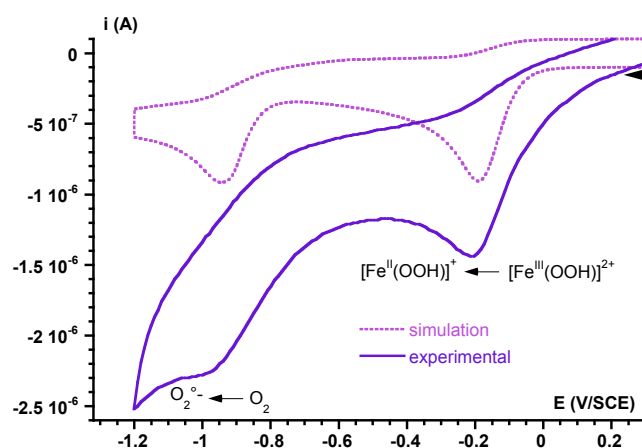


Figure S14. (Left) CV of complex **1** (1 mM in PrCN, 0.15 M TBAPF₆) at -70°C at various scan rates at a glassy carbon electrode. (Middle) Determination of the diffusion coefficient using Randles-Sevcik equation. (Right) Simulation of the CV at 0.1 V.s⁻¹ with E⁰(Fe^{III}/Fe^{II}) = 0.92 V, k⁰ = 0.003 cm.s⁻¹, D(**1**) = 4.5 10⁻⁷ cm².s⁻¹.

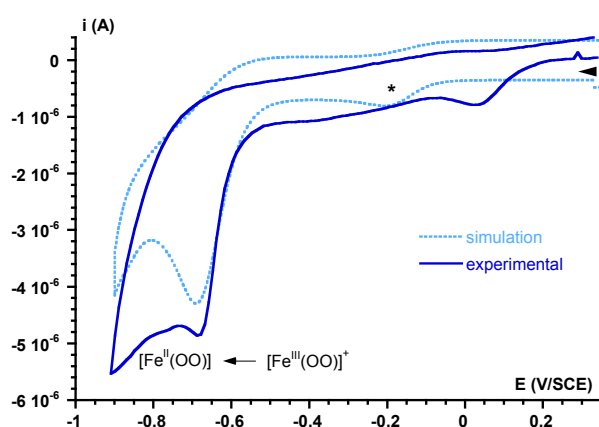
The value of the D coefficient obtained for **1** at 20°C (4.1 10⁻⁶ cm².s⁻¹) is identical to the one determined by Ségaud et al. for [Fe^{II}(TPEN)]²⁺ under the same conditions.⁹ This D value and k⁰ = 0.009 cm.s⁻¹ have been used for all Fe complex or reaction intermediate for the CV simulations of the **1** + O₂ reaction mixtures at 20°C. Indeed, experimental determination of these parameters for the [Fe^{III}(L₅²)(OOH)]²⁺ and [Fe^{III}(L₅²)(OO)]⁺ reaction intermediates is not possible as it is much longer than their lifetime. Considering that iron complexes of the same ligand display similar diffusion coefficient is a reasonable assumption.

As expected, the value of the D coefficient obtained for **1** at -70°C is much smaller. This D value (4.5 10⁻⁷ cm².s⁻¹) and k⁰ = 0.003 cm.s⁻¹ have been used for the simulation of the CVs the [Fe^{III}(L₅²)(OOH)]²⁺ and [Fe^{III}(L₅²)(OO)]⁺ reaction intermediates recorded at -70°C.



$[\text{Fe}^{\text{III}}(\text{OOH})]^{2+} + e^- \rightleftharpoons [\text{Fe}^{\text{II}}(\text{OOH})]^+$	$E^\circ = -0.20$	$k^\circ = 0.003$
$[\text{Fe}^{\text{II}}(\text{OOH})]^+ + [\text{Fe}^{\text{II}}(\text{OOH})]^+ \rightleftharpoons \text{A} + \text{O}_2$	$K = 1.0 \cdot 10^{10}$	$k_+ = 1.0 \cdot 10^{10}$
$\text{A} \rightleftharpoons [\text{Fe}^{\text{II}}(\text{OH})]^+ + [\text{Fe}^{\text{II}}(\text{OH})]^+$	$K = 1.0 \cdot 10^{10}$	$k_+ = 1.0 \cdot 10^{16}$
$\text{O}_2 + e^- = \text{O}_2^{\cdot -}$	$E^\circ = -0.89$	$k^\circ = 0.007$

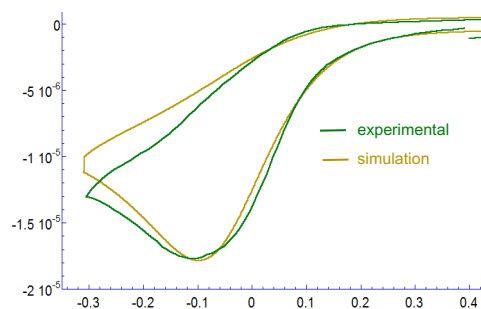
Figure S15. (Top) Experimental (purple line) and simulated (pink dotted line) CVs of $[\text{Fe}^{\text{III}}(\text{L}_5^2)(\text{OOH})]^{2+}$ (0.2 mM in PrCN, 0.2 M TBAPF₆) at -70°C at a glassy carbon electrode. The simulation has been obtained considering the reactions and parameters indicated at the bottom. These reactions correspond to reactions **E1**, **E5**, **C6** and **C7** in Mechanism C. E° values are given in V vs SCE, k° are in $\text{cm} \cdot \text{s}^{-1}$ and K units depend on the reaction order.



$[\text{Fe}^{\text{III}}(\text{OOH})]^{2+} + e^- \rightleftharpoons [\text{Fe}^{\text{II}}(\text{OOH})]^+$	$E^\circ = -0.20$	$k^\circ = 0.003$
$[\text{Fe}^{\text{III}}(\text{OO}^-)]^+ + e^- \rightleftharpoons [\text{Fe}^{\text{II}}(\text{OO}^-)]$	$E^\circ = -0.70$	$k^\circ = 0.003$
$[\text{Fe}^{\text{III}}(\text{OO}^-)]^+ + \text{H}_2\text{O} = [\text{Fe}^{\text{III}}(\text{OOH})]^{2+}$	$K_4 = 3.5 \cdot 10^5$	$k_+ = 1.0 \cdot 10^{14}$

Figure S16. (Top) Experimental (dark blue line) and simulated (dotted light blue line) CVs of $[\text{Fe}^{\text{III}}(\text{L}_5^2)(\text{OO})]^+$ (1.1 mM in PrCN, 0.2 M TBAPF₆) at -70°C at a glassy carbon electrode. The simulation was obtained by applying the three reactions and parameters indicated in the Table. These reactions correspond to reactions **E4**, **E5** and **C4** in Mechanism C. E° values are given in V vs SCE, k° are in $\text{cm} \cdot \text{s}^{-1}$, k_+ are in $\text{M}^{-1} \cdot \text{s}^{-1}$ and K units depend on the order of reactions.

The concentration of $[\text{Fe}^{\text{III}}(\text{L}_5^2)(\text{OOH})]^{2+}$ is fixed to 0 and the concentration of water is fixed to 2 mM to obtain the low intensity cathodic wave indicated by the asterisk, corresponding to the reduction of $[\text{Fe}^{\text{III}}(\text{L}_5^2)(\text{OOH})]^{2+}$ formed upon protonation of $[\text{Fe}^{\text{III}}(\text{L}_5^2)(\text{OO})]^+$. This wave displays the shape and intensity of the experimental one observed at 0 V, but not its potential. Thus, the cathodic wave at 0 V may also correspond to small amounts of degradation products such as oxo-bridged dinuclear species.



$[\text{Fe}^{\text{IV}}(\text{O})]^{2+} + e^- \rightleftharpoons [\text{Fe}^{\text{III}}(\text{O})]^+$	$E^\circ = -0.14$	$k^\circ = 0.009$
$[\text{Fe}^{\text{III}}(\text{O})]^+ + \text{H}_2\text{O} \rightleftharpoons [\text{Fe}^{\text{III}}(\text{OH})]^{2+}$	$K = 1 \cdot 10^5$	$k_+ = 1.0 \cdot 10^8$
$[\text{Fe}^{\text{III}}(\text{OH})]^{2+} + e^- = [\text{Fe}^{\text{II}}(\text{OH})]^+$	$E^\circ = -0.70$	$k^\circ = 0.009$

Figure S17. (Top) Experimental (dark green line) and simulated (light green line) CVs of $[\text{Fe}^{\text{IV}}(\text{L}_5^2)(\text{O})]^{2+}$ (1.1 mM in MeCN, 0.1 M TBAPF₆) at 20°C at various scan rates at a glassy carbon electrode. The simulation was obtained taking into account the three reactions and parameters indicated in the Table. E° values are given in V vs SCE, k° are in $\text{cm}^2 \cdot \text{s}^{-1}$, k_+ are in $\text{M}^{-1} \cdot \text{s}^{-1}$ and K units depend on the order of reactions. The value of the diffusion coefficient used is the one of complex **1** at 20°C ($D = 4.1 \cdot 10^{-6} \text{ cm}^2 \cdot \text{s}^{-1}$) is i

The reduction wave of $[\text{Fe}^{\text{IV}}(\text{L}_5^2)(\text{O})]^{2+}$ can be satisfactorily simulated considering an ECE mechanism as indicated in Figure S16. This ECE process is similar to the one reported for $[\text{Fe}^{\text{IV}}(\text{TPEN})(\text{O})]^{2+9}$ and $[\text{Fe}^{\text{IV}}(\text{N}_4\text{Py})(\text{O})]^{2+}$.¹⁴ No evidence of O-O cleavage in the $[\text{Fe}^{\text{III}}(\text{L}_5^2)(\text{OOH})]^{2+}$ or $[\text{Fe}^{\text{III}}(\text{L}_5^2)(\text{OO})]^+$ intermediates was obtained in this. Therefore, these reactions have not been considered in Mechanism C.

1 A. Bohn, C. Chinaux-Chaix, K. Cheaib, R. Guillot, C. Herrero, K. Sénéchal-David, J.-N. Rebilly and F. Banse, *Dalton Trans.*, 2019, **48**, 17045–17051.

2 M. Martinho, P. Dorlet, E. Rivière, A. Thibon, C. Ribal, F. Banse and J.-J. Girerd, *Chem. Eur. J.*, 2008, **14**, 3182–3188.

3 A. Thibon, V. Jollet, C. Ribal, K. Sénéchal-David, L. Billon, A. B. Sorokin and F. Banse, *Chem. Eur. J.*, 2012, **18**, 2715–2724.

4 J. J. Girerd, F. Banse and A. J. Simaan, *Struct. Bond.*, 2000, **97**, 145–177.

5 A. J. Simaan, F. Banse, P. Mialane, A. Boussac, S. Un, T. Kargar-Grisel, G. Bouchoux and J. J. Girerd, *Eur. J. Inorg. Chem.*, 1999, 993–996.

6 A. J. Simaan, S. Döpner, F. Banse, S. Bourcier, G. Bouchoux, A. Boussac, P. Hildebrandt and J.-J. Girerd, *Eur. J. Inorg. Chem.*, 2000, **2000**, 1627–1633.

7 D. F. Evans, *J. Chem. Soc.*, 1959, 2003–2005.

8 G. A. Bain and J. F. Berry, *J. Chem. Educ.*, 2008, **85**, 532.

9 N. Ségaud, E. Anxolabéhère-Mallart, K. Sénéchal-David, L. Acosta-Rueda, M. Robert and F. Banse, *Chem. Sci.*, 2015, **6**, 639–647.

10 J. M. Achord and C. Hussey, *Anal Chem*, 1980, **52**, 601–602.

11 M. Rudolph, *J. Electroanal. Chem.*, 2003, **543**, 23–39.

12 A. Bohn, K. Sénéchal-David, J. Rebilly, C. Herrero, W. Leibl, E. Anxolabéhère-Mallart and F. Banse, *Chem. A Eur. J.*, 2022, **28**, e202201600.

13 D. Wang, K. Ray, M. J. Collins, E. R. Farquhar, J. R. Frisch, L. Gómez, T. A. Jackson, M. Kerscher, A. Waleska, P. Comba, M. Costas and L. Que, *Chem. Sci.*, 2013, **4**, 282.

14 D. Wang, M. Zhang, P. Bühlmann and L. Q. Jr., *J. Am. Chem. Soc.*, 2010, **132**, 7638–7644.